Visually lossless coder for volumetric MRI and CT image data using wavelet transform

B.K. Chandrika

Department of Electrical and Electronics Engineering,
Manipal Institute of Technology,
Manipal University, India
Email: chandrika.bk@manipal.edu

P. Aparna and David S. Sumam*

Department of Electronics and Communication Engineering,
National Institute of Technology Karnataka,
Surathkal, India
Email: p.aparnadinesh@gmail.com
Email: sumam@ieee.org
*Corresponding author

Abstract: Medical imaging modalities produce large volume of digital data each day in modern healthcare. Several techniques have been proposed for volumetric medical image data compression. In this paper, we present a novel wavelet-based visually lossless coding scheme for the compression of volumetric magnetic resonance imaging (MRI) and computed tomography (CT) images. A visual model is incorporated in the coder to identify and measure visually irrelevant information. Performance of the compression scheme is further improved by eliminating the slice redundancy. The obtained results show better compression ratio compared to results obtained with pixel-based visually lossless compression technique, without any degradation in visual quality. We compared the performance of proposed technique with standard state of the art compression codecs such as joint photographic experts group-lossless (JPEG-LS), JPEG-2000, JPEG-3D, H.264/MPEG-4 AVC, differential pulse code modulation (DPCM) and medical image lossless compression (MILC). Results show better compression ratio over that of standard lossless compression schemes without any perceivable distortion.

Keywords: visually lossless image coding; visual model; MRI and CT images; quality metrics.

Reference to this paper should be made as follows: Chandrika, B.K., Aparna, P. and Sumam, D.S. (2017) 'Visually lossless coder for volumetric MRI and CT image data using wavelet transform', *Int. J. Computational Vision and Robotics*, Vol. 7, No. 6, pp.644–668.

Biographical notes: B.K. Chandrika is pursuing her PhD at National Institute of Technology Karnataka, Surathkal. She is an Assistant Professor at Department of Electrical and Electronics Engineering, Manipal Institute of Technology, Manipal University, Manipal. Her research interests are in the areas of image compression and digital system design.

P. Aparna received her PhD from National Institute of Technology Karnataka, Surathkal. She is an Assistant Professor at Department of Electronics and Communication Engineering, National Institute of Technology Karnataka. Her areas of interest include multimedia signal processing, biomedical signal processing and microprocessors and embedded systems.

David S. Sumam received her PhD from Indian Institute of Technology, Madras. She is a Professor at Department of Electronics and Communication Engineering, National Institute of Technology Karnataka. Her research interests include multimedia signal processing, signal compression, biomedical signal processing and VLSI architecture for signal processing.

1 Introduction

Volumetric medical image compression techniques play an important role in telemedicine and picture archiving and communication systems (PACS). It minimises the data storage requirement and the data transmission time leading to saving in transmission and PACS implementation cost. Number of three-dimensional (3D) images compression techniques that exploit the redundancies among pixel values of the image in the 3D space have been proposed so far. Among these, lossless solutions (Sanchez et al., 2009a, 2009b; Amraee et al., 2011) and wavelet-based lossy to lossless solutions providing quality and resolution scalability (Tzannes, 2003; Menegaz and Thiran, 2003; Bilgin et al., 2000) are preferred in medical applications. Even though these methods provide perfect reconstruction of image, they do not provide enough compression.

Lossy compression methods are another class of solutions available for the compression of 3D medical images (Ramaswamy and Mikhael, 1996; Gaudeau and Moureaux, 2009), providing lower bit rate than that of lossless coders at the cost of degradation in image quality. Quality of the reconstructed image is very critical as it may affect the diagnosis. An alternative solution to both the compression schemes is visually lossless coder (VLC), which discards visually irrelevant information along with other static redundancies present in 3D space of image to improve the compression ratio (Wu et al., 2006).

Magnetic resonance imaging (MRI), computed tomography (CT) and ultrasound are commonly used volumetric medical image acquisition systems as they support in detecting diseases or abnormalities in the body even though they generate huge data volume. Basically, human structural anatomy has approximate bilateral symmetry. This salient feature is reflected in axial and coronal view of MRI and CT images. Symmetry present in region of interest of MRI/CT image data and human visual perception feature can further improve the performance of algorithm (Chandrika et al., 2014).

This paper proposes a novel visually lossless compression scheme for MRI and CT image stack that embeds wavelet-based vision model with lossless image compression technique to remove visually redundant information. We choose a distortion metric based on human perception in order to measure the perceptually redundant information by exploiting the contrast and luminance masking properties of the human visual system (HVS).

Our scheme is based on a wavelet-based vision model that considers mixed masking effects of HVS to determine detection thresholds that change with the local frequency,

orientation and spatial features of the visual information such as contrast and luminance masking. The obtained thresholds are used to maintain the perceptual quality by eliminating only visually redundant information. Lossless compression techniques remove spatial and slice redundancies. Proposed algorithm attains minimum bit rate for a visually lossless target quality.

This paper is structured as follows: Section 2 briefly explains pixel-based visually lossless compression scheme in which contrast, luminance and texture masking properties are considered along with structural symmetry inherent in medical images. The proposed wavelet-based visually lossless compression scheme and vision model to retain the visual quality of original image is discussed in Section 3. Simulation is carried out on volumetric MRI and CT biomedical images. Details of medical images used to test the coding scheme and quality metrics used to evaluate the quality of reconstructed images are given in Section 4. Simulation results and comparison of proposed wavelet-based visually lossless scheme with pixel-based VLC, lossless compression algorithms such as differential pulse code modulation (DPCM), medical image lossless compression (MILC) and state of art compression standards such as JPEG 2000, JPEG 2000 part 2, JPEG 2000 part 10 (JP3D), joint photographic experts group-lossless (JPEG-LS), H.264/MPEG-4 AVC are reported in Section 5. Quality of the reconstructed image is evaluated through visual-based objective quality metrics.

2 Spatial domain visually lossless method

In this coding scheme, slice redundancy present in the image, symmetry nature of human anatomy and human visual characteristics are considered to compress the volumetric image data. Block diagram of the proposed method is illustrated in Figure 1. Visibility threshold value is calculated first using spatial domain-based just noticeable distortion (JND) model for all image slices. Parallely, presence of symmetry in each image slice is determined. Based on the visibility threshold value perceptually redundant information is removed using quantiser. On the resulting image slices, block matching algorithm is applied to remove inter-slice redundancy. Intra block match routine is applied on residual data of each slice to improve bit rate if symmetry is present in the image plane. The image residue generated by the block matching algorithm and displacement vectors are compressed using arithmetic coding.

- *Pixel-based visual model*: To reconstruct an image of high visual quality with good compression ratio, image compression algorithm should not only eliminate the numerical redundancies but also the visually insignificant contents from the image data. JND profile is employed to assess the perceptual redundancy by considering features of HVS and it provides a visibility threshold of distortion for each pixel in an image below which reconstruction errors are unnoticeable. In this work, pixel-based JND model (Yang et al., 2005) has been selected. Perceptual redundancies present in images are primarily due to the disparity in sensitivity of the HVS to the differing levels of contrast and luminance variation in the spatial domain.

  Third factor is the edge accommodative texture masking in spatial domain, added to handle the HVS characteristic better. An increase in the texture heterogeneity in the background will accommodate more reduction in the visibility of distortion. Accordingly, textured area can mask more deformity than smooth regions. Also,

error inserted in edge regions is more prominent compared to non-edge areas due to the reality that edge texture drags more attention from a classic HVS. This model explores both edge and non-edge regions along with luminance masking and texture masking.

- *Inter-slice and intra-slice block matching*: Medical image slices generated by imaging modalities are generally cross sections of human body and all the slices are parallel to one another. So there is correlation between adjacent image slices. Inter-slice block matching routine is used to improve bit rate by removing the redundancies in slice direction. Current image slice, I_i, is split into non-overlapped blocks of 8 × 8. 16 × 16 search window is defined in the previous image slice, I_{i-1}. Since there is correlation between the two successive image slices there must be a best match for each 8 × 8 block in search window. Minimum value of sum of absolute difference decides the best match. Corresponding block matching error and displacement vector is taken for further processing. Intra-slice block matching is same as inter-slice block matching routine.
- *Symmetry detection*: Human body has bilateral symmetry. This inherent feature is preserved in most of the medical image slices. Function of symmetry detector in this compression algorithm is to determine prominent axis of bilateral symmetry (Loy and Eklundh, 2006). Symmetry-based image compression method takes advantage of this bilateral symmetry in the medical images to improve the compression further. Intra-slice block matching step is bypassed in case, there is no bilateral symmetry.
- *Arithmetic coding*: Arithmetic coding is one of the entropy coding methods used in lossless data compression. In entropy coding, frequently occurring symbols are encoded with fewer bits and not-so-frequently occurring symbols are encoded with more bits. Huffman code translates each symbol of the message into a series of bits, while arithmetic code overcomes this disadvantage by encoding the entire message into one number. Arithmetic coding tries to evaluate the probability with which certain characters appear and optimises the length of the code. Another advantage of arithmetic coding over other entropy coders is the convenience of adaptation, i.e., update of probability tables as the data is processed. Due to all these advantages, we applied adaptive arithmetic coding in this work, to encode image residuals obtained after applying block matching algorithm.

Figure 1 Block diagram of pixel-based VLC scheme

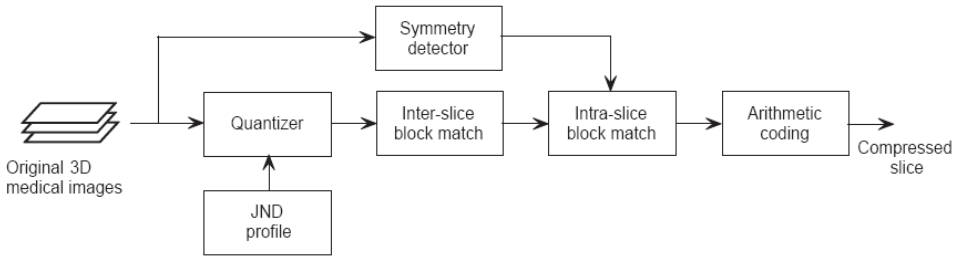

3 Wavelet-based VLC

The block diagram of the proposed wavelet-based visually lossless compression technique for volumetric medical data is illustrated in Figure 2. The slice redundancy and human visual characteristics are considered to compress the volumetric image data. Each image is first decomposed with 2D discrete wavelet transform (DWT) for n frequency levels. A wavelet-based vision model is used to measure the JND followed by a JND dependent quantiser to remove visually irrelevant information. On the resulting image slices, block matching algorithm is applied to remove inter-slice redundancy. The image residue generated by the block matching algorithm and displacement vectors are compressed using arithmetic coding.

Figure 2 Block diagram of wavelet-based VLC

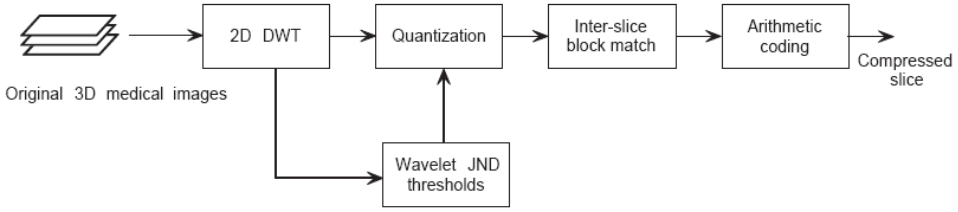

3.1 2D DWT

The basic principle of the 2D DWT is to represent a 2D signal as a superposition of a wavelet basis. The coefficients of the basis can then be utilised to reconstruct the original information. The 2D DWT gives frequency and spatial representation of 2D signals. Each frequency level of the transform decomposes its input into four spatial frequency subbands denoted as LL, LH, HL and HH. The orientations are indexed as 1, 2, 3, 4 corresponding to the LL, HL, HH and LH subbands, respectively. The approximation low pass subband LL, is a coarser version of the original signal, while the other subbands represent the high frequency details in the horizontal, vertical and diagonal directions, respectively. The decomposition is usually iterated on the approximation low pass subband, which for natural images contains most of the energy. The wavelet transform has many features that make it suitable for our application, such as representation of an image at different resolutions and packing of most of the energy in a few wavelet coefficients.

3.2 JND thresholds for wavelet coefficients

In this stage, the perceptual redundancy present in image is measured through JND profile. The visual model uses one JND threshold, $v_{JND}(l, \theta, [m, n])$ for every DWT coefficient at location $[m, n]$ in subband (l, θ),where l is the frequency level and θ is the orientation. In this work, three important visual characteristics are modelled to determine the JND thresholds (Liu et al., 2006) namely contrast sensitivity, luminance masking or light adaption and contrast masking. The JND threshold $v_{JND}(l, \theta, [m, n])$ is thus computed as

$$v_{JND}\left(l,\theta,[m,n]\right) = JND_{(l,\theta)}a_l\left(l,\theta,[m,n]\right)a_c\left(l,\theta,[m,n]\right) \tag{1}$$

where $JND_{(l,\theta)}$ is the base detection threshold of a subband (l, θ), $a_l(l, \theta, [m, n])$ is the light adaptation adjustment and $a_c(l, \theta, [m, n])$ is the contrast masking adjustment.

The base detection threshold $JND(l, \theta)$ for each subband (l, θ) provides the relative variation in the visible signal over a background with uniform intensity. Contrast is an essential theory in vision science because the response of the HVS depends on the variation of the signal relative to the surround background instead of absolute luminance value.

A mathematical representation of JND threshold is given by (Liu et. al. (2006)

$$JND_{(l,\theta)} = \frac{a10^{k\left\{\log\left(\frac{g_\theta f 2^l}{r}\right)\right\}^2}}{A_{l,\theta}} \tag{2}$$

where a, k, f, r and g_θ are constants and obtained with a background intensity of 128. Values of these constants are listed in Table 1. $A_{l,\theta}$ is the amplitude of the DWT 9/7 kernel basis function. Its value depends on frequency level l, orientation θ and visual resolution of the display in pixels/degree r. Table 2 lists the $A_{l,\theta}$ values for a 5-level 9/7DWT decomposition (Liu et al., 2006). The base detection threshold values change with the background intensity levels. Hence, mean luminance of the local image region needs to be considered when calculating detection threshold. Therefore, to account for this variation a luminance masking correction factor must be applied to the contrast sensitivity function. The luminance masking adjustment is approximated as:

$$a_l\left(l,\theta,[m,n]\right) = \left(\frac{c\left(l_{\max}, LL, [m', n']\right)}{c_{mean}}\right)^{a_T} \tag{3}$$

where $c(l_{\max}, LL, [m', n'])$ is the value of the DWT coefficient, in the LL subband, that spatially corresponds to position (l, θ, [m, n]). In this case, m' and n' can be calculated as $m' = \left\lfloor \frac{m}{2^{l_{\max}-l}} \right\rfloor$ and $n' = \left\lfloor \frac{m}{2^{l_{\max}-l}} \right\rfloor$. The parameter a_T controls luminance masking, a value of 0.649 was used.

Table 1 Parameters for the DWT threshold model

a	k	f	g_{LL}	$g_{HL,LH}$	g_{HH}	r (pixels/degree)
0.495	0.466	0.401	1.501	1.0	0.534	35

Source: Liu et al. (2006)

Table 2 Basis function amplitude $A_{l,\theta}$ for a 5 level 9/7 DWT

Orientation	*DWT*				
	1	*2*	*3*	*4*	*5*
LL	0.62171	0.34537	0.18004	0.09140	0.045943
LH,HL	0.67234	0.413177	0.22727	0.11792	0.059758
HH	0.72709	0.49428	0.28688	0.15214	0.077727

Source: Liu et al. (2006)

Contrast masking is another factor that will affect the detection threshold. It is due to the fact that the visibility of one image component changes with the presence of another image component (Chou and Li, 1995). Contrast masking estimates the variation of the detection threshold in a target signal as a function of the contrast of the masker. The contrast masking effect can be framed as:

$$a_{c\_}\left(l,\theta,[m,n]\right)=a_{c\_self}\left(l,\theta,[m,n]\right)a_{c\_neigh}\left(l,\theta,[m,n]\right) \tag{4}$$

where $a_{c\_self}(l, \theta, [m, n])$ is the self contrast masking adjustment factor and $a_{c\_neigh}(l, \theta, [m, n])$ is the neighbourhood contrast masking adjustment factor.

A sufficiently large coefficient at the location $(l, \theta, [m, n])$ increases the detection threshold. This variation in detection threshold is incorporated through self contrast masking adjustment factor $a_{c\_self}(l, \theta, [m, n])$. For the DWT coefficients, it is expressed as:

$$a_{c\_self}\left(l,\theta,[m,n]\right)=\max\left\{1,\left(\frac{\left|c\left(l,\theta,[m,n]\right)\right|}{JND_{(l,\theta)}a_l\left(l,\theta,[m,n]\right)}\right)^{\varepsilon}\right\} \tag{5}$$

where $c(l, \theta, [m, n])$ is the DWT coefficient value at location $(l, \theta, [m, n])$. For the LL subband, contrast masking is not applied ($\varepsilon = 0$). For other subbands, ε is 0.6.

In DWT-based reconstructed images, the signal formed by DWT coefficient $c(l, \theta, [m, n])$ is superimposed on other signals formed by the neighbouring wavelet coefficients. This phenomena is taken in to account through neighbourhood contrast adjustment factor $a_{c\_neigh}(l, \theta, [m, n])$. So there is some masking effect contributed from spatially neighbouring signals in wavelet domain. It is expressed as (Liu et al., 2006):

$$a_{c\_neigh}\left(l,\theta,[m,n]\right)=\max\left\{1,\sum_{k\in neighbours\ of\ (l,\theta,[m,n])}\frac{\left|\frac{c_k}{JND_{(l,\theta)}a_l\left(l,\theta,[m,n]\right)}\right|^{\zeta}}{N_{[m,n]}}\right\} \tag{6}$$

where the neighbourhood contains the coefficients in the same subband that lie within a window centred at the location $[m, n]$. $N_{[m,n]}$ represents the number of coefficients in that neighbourhood. c_k are the neighbouring wavelet transform coefficient values. $\zeta = 0.5$ is a constant that controls the influence of the amplitude of each neighbouring coefficient.

3.3 JND dependent quantiser

This section explains the approach to eliminate perceptual redundancies to reduce the bit rate of the coding scheme. The most simple approach of eliminating the visually redundant information from DWT coefficients is to quantise the DWT coefficients in such a way that absolute value of quantisation error is below the JND value. After evaluating the image dependent JND value, each reference or original DWT coefficient $c(l, \theta, [m, n])$ is quantised to get $cd(l, \theta, [m, n])$ through truncation of $c(l, \theta, [m, n])$. So

$$cd_k\left(l,\theta,[m,n]\right)=\left\lfloor\frac{c\left(l,\theta,[m,n]\right)}{k}\right\rfloor\times k \tag{7}$$

where $\lfloor\ \rfloor$ is the truncation function and k is an integer. Finally, if the quantised DWT coefficient $cd_k(l, \theta, [m, n])$ is below the JND threshold $v_{JND}(l, \theta, [m, n])$, the reference DWT coefficient $c(l, \theta, [m, n])$ at location $[m, n]$ is replaced by the corresponding quantised DWT coefficient $cd_k(l, \theta, [m, n])$. The pseudo code of this procedure is shown in Figure 3, where $cv(l, \theta, [m, n])$ is visually lossless DWT coefficient.

- *Inter slice block matching*: Inter-slice block matching routine is applied separately for different subbands to exploit correlation between adjacent image slices.

Figure 3 Pseudo code for eliminating visual redundancy

Procedure for eliminating visual redundancy:

$cv(l, \theta, [m, n]) = c(l, \theta, [m, n]);$

for k=4:2

$cd_k(l, \theta, [m, n]) = \lfloor \frac{c(l, \theta, [m, n])}{k} \rfloor \times k;$

if $| c(l, \theta, [m, n]) - cd_k(l, \theta, [m, n]) | \leqslant v_{JND}(l, \theta, [m, n])$ *then*

$cv(l, \theta, [m, n]) = cd_k(l, \theta, [m, n]);$

break

end if

end for

4 Implementation

The proposed method has been simulated using MATLAB® on an Intel® core i3-2120 processor at 3.3GHz. Performance of the wavelet-based and pixel-based VLC for volumetric medical image sets are compared with few of the standard image compression codecs. The coder is developed for a viewing distance of 24 inches (approximately arm's length) and for a display with around 35 pixels/degree display visual resolution. DWT is implemented with 9/7 wavelet filter with frequency level of 5. The value of parameters a, k, f, r and g_θ used in the JND model are based on the experiment carried with various models to express the threshold for gray scale DWT noise as a function of spatial frequency and orientation θ (Watson et al., 1997).

4.1 Medical image dataset

We evaluate wavelet-based and pixel-based VLC on 251 number of 8 bit MR image slices and 557 number of CT image slices from Mallinckrodt Institute of Radiology, Image processing Laboratory (Bilgin et al., 2000). Details of these image datasets are summarised in Table 3 and selected image slice from each dataset is shown in Figure 4.

Table 3 Details of the volumetric medical images used in the assessment

Image	*Label*	*Resolution (W × H × D) (in pixel)*	*Dynamic range (bpp)*	*Voxel dimensions (mm)*	*History*
CT skull	CT1	256 × 256 × 203	8	0.7 × 0.7 × 2	Tripod fracture
CT wrist	CT2	256 × 256 × 183	8	0.17 × 0.17 × 2	Healing scaphoid dissection
CT carotid	CT3	256 × 256 × 74	8	0.25 × 0.25 × 1	Internal carotid dissection
CT aperts	CT4	256 × 256 × 97	8	0.35 × 0.35 × 2	Aperts syndrome
MRI liver t1	MR1	256 × 256 × 58	8	1.45 × 1.45 × 5	Normal
MRI liver t2	MR2	256 × 256 × 58	8	1.37× 1.37 ×5	Normal
MRI Sag head	MR3	256 × 256 × 58	8	0.98× 0.98 ×3	Left exophthalmos
MRI Ped chest	MR4	256 × 256 × 77	8	0.78× 0.78 ×5	Congenital heart disease

Source: Bilgin et al. (2000)

Figure 4 Selected image slices from each of the image set, (a) CT skull (CT1) (b) CT wrist (CT2) (c) CT carotid (CT3) (d) CT aperts (CT4) (e) MRI liver t1 (MR1) (f) MRI liver t2 (MR2) (g) MRI Sag head (MR3) (h) MRI Ped chest (MR4)

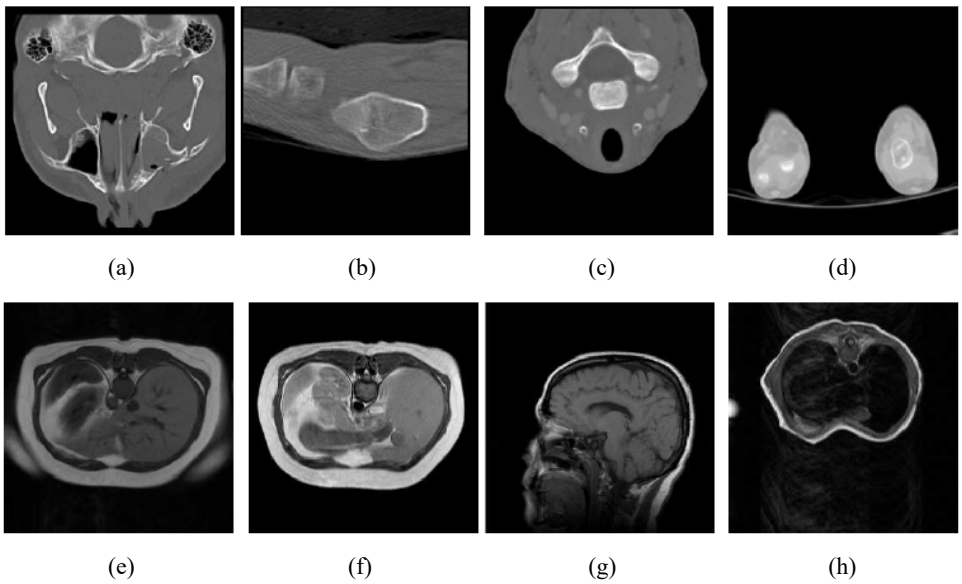

(a) (b) (c) (d)

(e) (f) (g) (h)

4.2 Metrics for evaluating compression algorithms

Both objective and subjective quality measures are used to assess the compression algorithms. Quantitative performance metrics such as peak signal to noise ratio (PSNR) and relative error (RE) are commonly employed error measures to analyse the original and the reconstructed image in case of lossy compression techniques even though many a time they do not correlate well with subjective quality sensed by the HVS. Visual signal to noise ratio (VSNR), visual information fidelity (VIF) and structural similarity index (SSIM) are some of the HVS-based quantitative performance metrics available in literature to evaluate the quality of the reconstructed image followed by lossy compression for natural images. These statistical metrics are applied to evaluate the perceptually lossless coding algorithms since they closely emulate the HVS. Range of the quantitative quality metrics are tabulated in Table 4.

VSNR (Chandler and Hemami, 2007) operates via two stage approach. In the first stage, contrast detection threshold is computed with wavelet-based models of visual masking and visual summation to determine the visibility of distortion in the distorted image. If the distortions are below the threshold of detection, then VSNR = ∞. If the distortions are above the threshold, VSNR value is calculated.

Table 4 Range of quantitative quality metrics

Metric	*Range*	*Value for perfect quality*
PSNR (dB)	0 to ∞	∞
VSNR (dB)	0 to ∞	∞
SSIM	0 to 1	1
VIF	0 to 1	1
RE	1 to 0	0

VSNR is defined as:

$$VSNR = 20\log_{10}\left(\frac{C(I)}{C(E)}\right) \tag{8}$$

where $C(I)$ denotes the RMS contrast of the original image I and $C(E)$ denotes the RMS contrast of the reconstructed image.

SSIM (Wang et al., 2004) compares the brightness, contrast and structure between original and reconstructed image. It has been proved through receiver operating characteristic analysis that SSIM provides a closer match to subjective assessments (Kowalik-Urbaniak et al., 2014).

Expression for SSIM between two signals x and y is given by the following expression

$$SSIM(x, y) = \frac{\left(2\mu_x\mu_y + C_1\right)\left(2\mu_{xy} - \mu_x\mu_y + C_2\right)}{\left(\mu_x^2 + \mu_y^2 + C_1\right)\left(\sigma_x^2 + \sigma_y^2 + C_2\right)} \tag{9}$$

where μ_x is the average intensity of signal x, μ_y is the average intensity of signal y, σ_x is the standard deviation of x, σ_y is the standard deviation of y, C_1 and C_2 are constants.

VIF (Sheikh and Bovik, 2006) quality measure is based on correlation distortion, contrast distortion, and luminance distortion. In this quality assessment, the amount of information can be extracted by brain from the original image is first measured. Later, loss of the same information in the presence of reconstructed image is measured.

5 Results and discussion

5.1 Impact on performance of coder with and without neighbourhood masking

The influence of considering neighbourhood contrast adjustment along with self contrast adjustment with different bit rates as discussed in Section 3.2 is shown in Figure 5. Table 5 compares quality metrics such as PSNR and VIF against the bit rate for VLC considering only self masking and VLC considering both self and neighbourhood masking. For almost same quality, VLC with both masking gives reduced bit rate. There is an overall improvement in bit rate by 7.89%. Although VLC with neighbourhood contrast adjustment increases the computation complexity, there is gain in compression ratio. So we have considered both self and neighbourhood masking for the results reported.

Table 5 Bit rate and quality metrics of reconstructed image with and without neighbourhood masking

Label	*Self masking*				*Self and neighbourhood masking*			
	bpp	*PSNR (dB)*	*VSNR (dB)*	*VIF*	*bpp*	*PSNR (dB)*	*VSNR (dB)*	*VIF*
CT1	1.540	50.85	45.51	0.945	1.420	50.76	45.69	0.943
CT2	0.807	52.59	52.72	0.941	0.737	52.53	52.75	0.941
CT3	1.160	52.35	49.94	0.95	1.123	52.33	49.94	0.95
CT4	0.715	54.94	56.30	0.959	0.660	54.91	56.33	0.959
MR1	1.389	49.66	45.38	0.94	1.290	49.62	45.39	0.939
MR2	1.208	51.82	46.34	0.958	1.178	51.81	46.34	0.958
MR3	1.440	51.16	52.72	0.93	1.284	51.10	52.74	0.928
MR4	1.123	50.03	55.60	0.913	0.957	49.94	55.68	0.911

We have performed these simulations considering 9/7 wavelet filter and frequency level of 5. We have used Biorthogonal 9/7 wavelet filter set as it gives very good compression and has been used extensively in image compression applications (Villasenor et al., 1995). Generally, as the number of decomposition levels is increased coding efficiency improves and it has been shown that most of the coding efficiency is contributed by the first three to five decomposition levels beyond which the efficiency levels off (Adams and Ward, 2001). Hence, 5-level decomposition is chosen.

Figure 5 Comparison of bit rate for all medical image datasets with and without neighbourhood masking

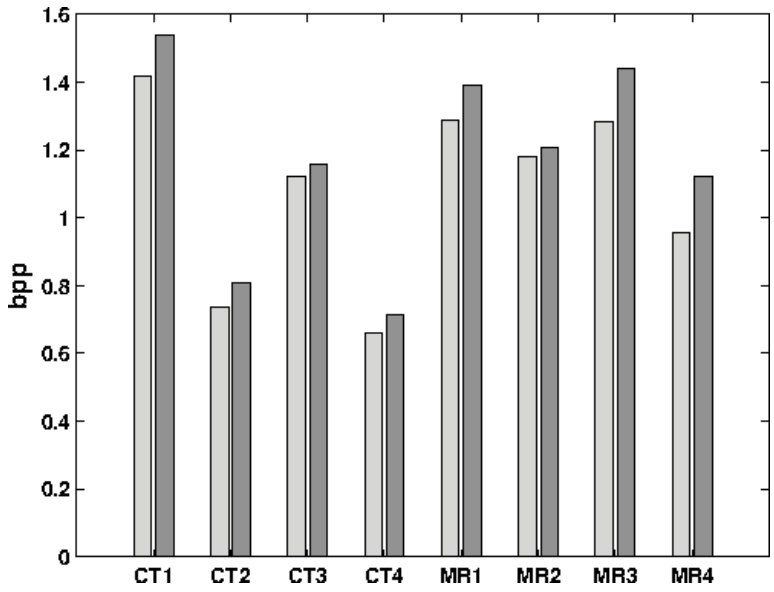

5.2 Effect of frequency levels in DWT

It is important to check the effect of decomposition levels in DWT on visually lossless compression ratio. As mentioned in Section 3.2, basis function amplitude $A_{l,\theta}$ is not same for different frequency levels of DWT and hence, the JND values. The pseudo code for quantising the DWT coefficients to get undistorted image is given in Figure 3. In this case image is decomposed using 9/7 wavelet filter bank. As the number of levels of decomposition in DWT increases it is possible to represent the data in more redundant form. So higher levels of decomposition should provide better compression ratio. Our results in Figure 6 reconfirm this fact.

Table 6 Comparison of visually lossless bit rate (bpp) and VIF of reconstructed image for wavelet decomposition levels 1 to 5

Label	*Wavelet-based (Daub 9/7)VLC*				
	Level-1	*Level-2*	*Level-3*	*Level-4*	*Level-5*
CT1	2.156/0.958	2.064/0.951	1.928/0.949	1.747/0.947	1.540/0.945
CT2	1.290/0.967	1.231/0.950	1.040/0.947	0.914/0.943	0.807/0.941
CT3	1.744/0.97	1.656/0.958	1.427/0.95	1.218/0.95	1.160/0.95
CT4	1.173/0.978	1.190/0.970	1.032/0.966	0.833/0.960	0.715/0.959
MR1	2.324/0.96	2.293/0.95	1.981/0.945	1.657/0.94	1.389/0.94
MR2	1.744/0.965	1.585/0.96	1.4/0.958	1.27/0.958	1.208/0.958
MR3	2.187/0.95	2.259/0.944	2.092/0.94	1.829/0.93	1.44/0.93
MR4	1.873/0.949	1.887/0.938	1.677/0.928	1.411/0.919	1.123/0.913

The average reduction in bit rate from level 1 to level 5 is 35.46% considering all four sets of CT and four sets of MR images. Table 6 compares the bit rate (bpp) and VIF across the different levels. For different frequency levels, bit rate (bpp) and PSNR (dB) comparison is given in Table 7. Similarly, bpp and VSNR (dB) for various levels are given in Table 8. Tabulated PSNR, VIF and VSNR values for levels 1 to 5 demonstrate that there is no perceivable distortion by increasing the frequency level since there is not much difference in quality metrics from frequency levels 1 to 5.

Figure 6 Comparison of VLC bit rate for frequency levels from 1 to 5 with all test datasets

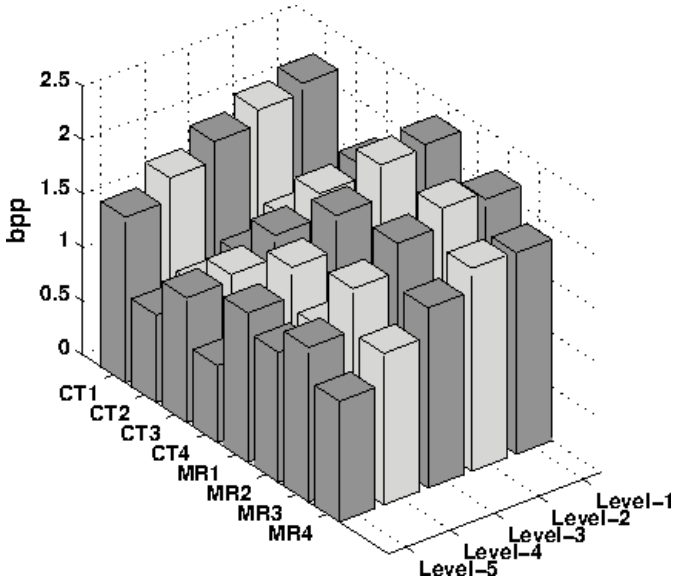

Table 7 Comparison of visually lossless bit rate (bpp) and PSNR (in dB) of reconstructed image for wavelet decomposition levels 1 to 5

Image set	*Wavelet-based (Daub 9/7)VLC*				
	Level-1	*Level-2*	*Level-3*	*Level-4*	*Level-5*
CT1	2.156/52.07	2.064/51.39	1.928/51.28	1.747/51.11	1.54/50.85
CT2	1.29/54.85	1.231/53.23	1.040/52.90	0.914/52.70	0.807/52.59
CT3	1.744/54.16	1.656/52.96	1.427/52.60	1.218/52.39	1.160/52.35
CT4	1.173/57.43	1.190/56.30	1.032/55.70	0.833/55.13	0.715/54.94
MR1	2.324/51.63	2.293/50.57	1.981/50.12	1.657/49.82	1.389/49.66
MR2	1.744/52.83	1.585/52.15	1.400/51.95	1.270/51.86	1.208/51.82
MR3	2.187/52.59	2.259/52.21	2.092/51.85	1.829/51.48	1.440/51.16
MR4	1.873/52.12	1.887/51.13	1.677/50.74	1.411/50.33	1.123/50.03

Table 8 Comparison of visually lossless bit rate (bpp) and VSNR (in dB) of reconstructed image for wavelet decomposition levels 1 to 5

Image set	*Wavelet-based (Daub 9/7) VLC*				
	Level-1	*Level-2*	*Level-3*	*Level-4*	*Level-5*
CT1	2.156/45.37	2.064/45.52	1.928/45.33	1.747/45.37	1.540/45.51
CT2	1.290/53.29	1.231/52.72	1.040/52.67	0.914/52.68	0.807/52.72
CT3	1.744/50.24	1.656/50.06	1.427/49.96	1.218/49.94	1.160/49.94
CT4	1.173/65.07	1.190/56.39	1.032/56.13	0.833/56.11	0.715/56.30
MR1	2.324/45.90	2.293/45.59	1.981/45.42	1.657/45.37	1.389/45.38
MR2	1.744/46.73	1.585/46.58	1.400/46.36	1.270/46.37	1.208/46.34
MR3	2.187/52.41	2.259/52.54	2.092/52.43	1.829/52.59	1.440/52.72
MR4	1.873/55.45	1.887/55.55	1.677/55.42	1.411/55.44	1.123/55.60

5.3 Comparison of VLC performance with type of wavelet filter

We also test the impact of wavelet filters on bit rate and visual quality of reconstructed image. Table 9 compares the performance of VLC with 9/7 wavelet kernel and 5/3 wavelet kernels. For the visually lossy compression, 9/7 wavelet kernel performs better than 5/3 wavelet kernel. For the same image quality 9/7 wavelet kernel improves the compression by 35.16%.

Table 9 Comparison of visually lossless bit rate (bpp) and PSNR (dB) with 9/7 and 5/3 kernels

Label	*With wavelet 9/7 kernel*	*With wavelet 5/3 kernel*
CT1	0.99/40.88	1.42/39.95
CT2	0.54/44.05	0.84/41.66
CT3	0.62/42.99	0.968/41.29
CT4	0.64/44.42	1.06/44.42
MR1	0.8/41.84	1.36/39.19
MR2	0.75/40.81	1.02/40.52
MR3	0.92/41.66	1.29/41.07
MR4	0.73/42.32	1.29/40.33

5.4 Comparison of VLC with pixel-based and wavelet-based JND model

We compared the performance of VLC with pixel-based visual model explained in Section 2 and the wavelet-based visual model of Section 3. Pixel-based visual model is dependent on average background luminance, spatial luminance gradient and texture masking. It does not decompose image into different frequency levels to represent in more redundant form like wavelet-based approach. So wavelet-based VLC performs better than pixel-based coder. Table 10 demonstrates this fact and we observed a reduction in bit rate by 30.01% in case of wavelet-based vision model against pixel-based VLC.

Table 10 Comparison of visually lossless bit rate (bpp) and PSNR (dB) corresponding to pixel-based and wavelet-based visual model

Image	*Pixel-based model*	*Wavelet-based model*
CT1	1.6529/50.42	1.51/50.79
CT2	1.1377/49.05	0.65/49.46
CT3	1.5087/52.46	1.15/52.31
CT4	0.7777/50.28	0.77/50.51
MR1	2.2828/42.67	0.81/42.65
MR2	1.7918/51.20	1.2/51.79
MR3	1.5588/46.42	1.18/47.60
MR4	1.3363/43.32	0.75/43.52

5.5 Comparison of VLC with lossless codes and image compression standards

Performance of VLC, standard codecs and lossless compression algorithms for the test medical image data base is given in Table 11. Wavelet-based VLC is compared with the state of art codecs such as JPEG-LS (JPEG-LS), JPEG2000 (JPEG-2000), JPEG3D (JPEG 3D) image coding standard, H.264/MPEG-4 AVC (H.264/AVC) video coding, DPCM (Ait-Aoudia et al., 2006) and MILC (Pizzolante and Carpentieri, 2013) lossless compression algorithms.

Table 11 Comparison of visually lossless bit rates obtained with lossless bit rates of JPEG-2K, JPEG-LS, JPEG3D, H.264/MPEG-4 AVC, DPCM and MILC

Label	*Wavelet-based VLC**	*JPEG2000*	*JPEG-LS*	*JPEG-3D*	*H.264/ MPEG-4 AVC*	*DPCM*	*MILC*
CT1	1.42/50	2.955	2.728	2.120	1.967	2.119	2.030
CT2	0.73/49.98	1.897	1.607	1.258	1.150	1.029	1.066
CT3	1.12/49.73	2.366	1.756	1.567	1.539	1.471	1.358
CT4	0.715/50.51	1.245	1.044	0.969	0.819	0.867	0.819
MR1	1.29/49.66	3.254	3.167	2.379	2.319	2.390	2.196
MR2	1.17/51.82	2.541	2.388	1.778	1.769	2.025	1.759
MR3	1.44/51.16	3.952	2.551	2.188	2.015	2.127	2.097
MR4	1.12/51.59	2.985	2.901	2.131	1.762	1.689	1.655

Note: *Bit rate (bpp)/mean PSNR (dB)

JPEG-LS is a near lossless/lossless compression standard for natural images and is based on prediction, residual modelling and context-based coding of the residuals (Weinberger et al., 2000). JPEG2000 (JPEG2ISO: International Organization for Standardisation, 1999) is the still image compression standard and it is used in Digital Imaging and Communications in Medicine (DICOM) standard. JPEG2000 employs 2D integer wavelet transform. JPEG3D is the extension of JPEG2000 standard codec (JPEG3DISO: International Organization for Standardisation, 2002). It employs DWT across the slices and applies JPEG2000 on the resulting transform slices. H.264/MPEG-4 AVC is a standard codec for the compression of video (Marpe et al., 2006). It employs multi frame motion compensation and estimation.

In case of proposed VLC, visually lossless bit rates are obtained by setting the value of k to 3 [equation (7)] in the process of eliminating the visual redundancy. On 8 bit MR and CT images, wavelet-based VLC improves compression by 60.07% compared with JPEG2000; 48.17% compared with JPEG-LS; 36.41% compared with JPEG-3D, 30.92% compared with H.264/MPEG-4 AVC, 32.20% compared with DPCM and 28.76% compared with MILC. Figure 7 shows reconstructed images with our VLC for the selected image slices given in Figure 4.

Figure 7 Reconstructed images corresponding to image slices given in Figure 4, (a) CT skull (CT1) (b) CT wrist (CT2) (c) CT carotid (CT3) (d) CT aperts (CT4) (e) MRI liver t1 (MR1) (f) MRI liver t2 (MR2) (g) MRI Sag head (MR3) (h) MRI Ped chest (MR4)

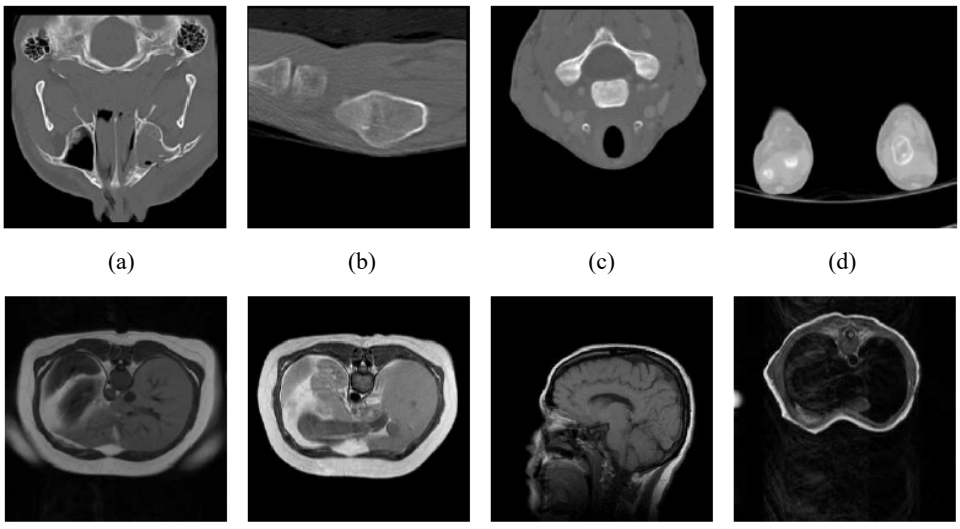

(a) (b) (c) (d)

(e) (f) (g) (h)

Figure 8 Visual clip of CT Skull and MRI Liver t1: (a) CT Skull at bpp of 1.89 and PSNR = 51.22 dB (b) CT skull at bpp of 1.06 and PSNR = 42.47 dB (c) MRI liver t1 at bpp of 2.06 and PSNR = 49.52 dB (d) MRI liver t1 at bpp of 0.84 and PSNR = 43.63 dB

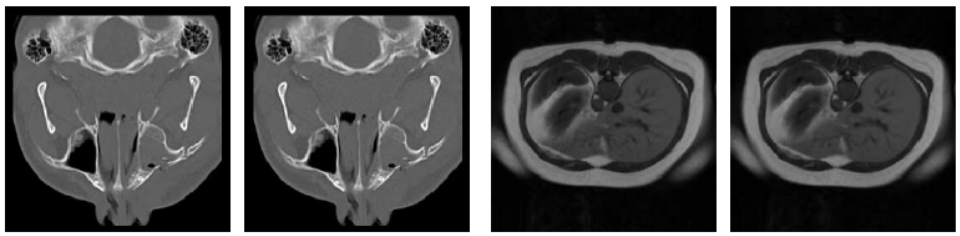

(a) (b) (c) (d)

Figure 9 Comparison of PSNR (in dB) as a function of bit rate (bpp) for VLC with JPEG 2000 Part 1 (JP-2KP1) and JPEG 2000 Part 2 (JP-2KP2), (a) CT skull (b) CT wrist (c) MRI liver t1 (d) MRI Ped chest (see online version for colours)

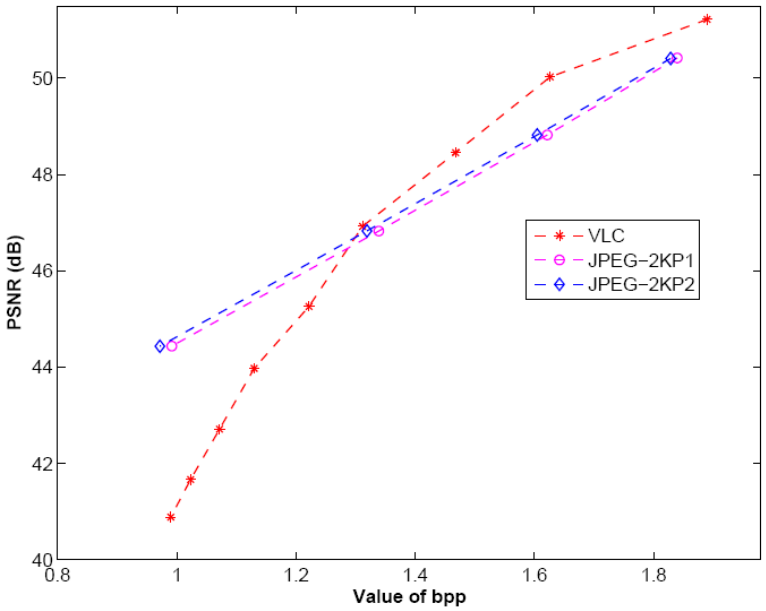

(a)

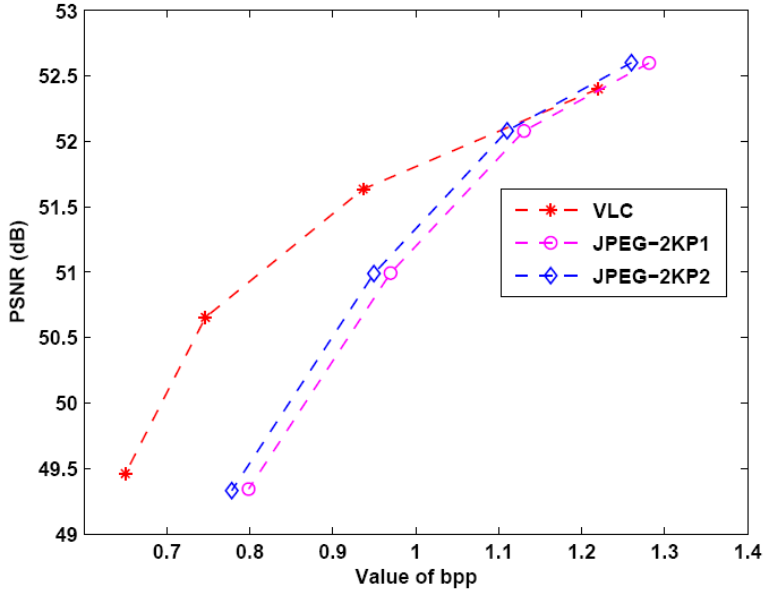

(b)

Figure 9 Comparison of PSNR (in dB) as a function of bit rate (bpp) for VLC with JPEG 2000 Part 1 (JP-2KP1) and JPEG 2000 Part 2 (JP-2KP2), (a) CT skull (b) CT wrist (c) MRI liver t1 (d) MRI Ped chest (continued) (see online version for colours)

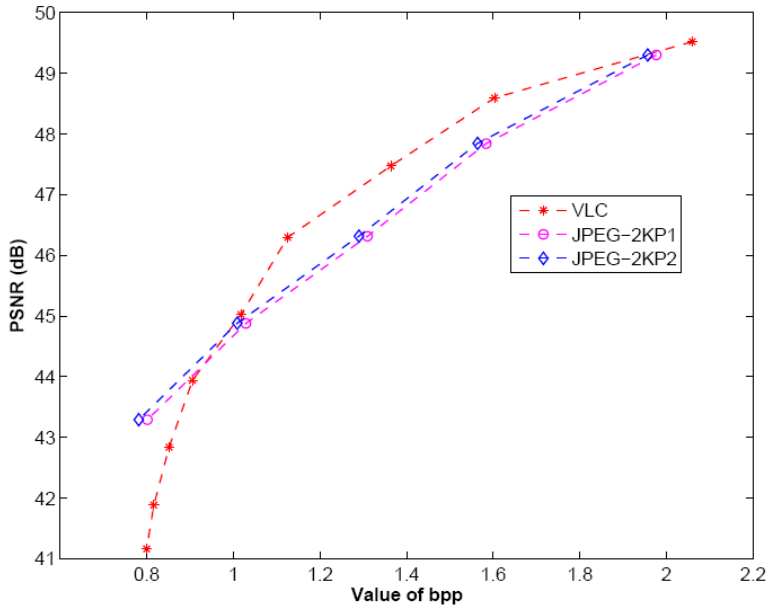

(c)

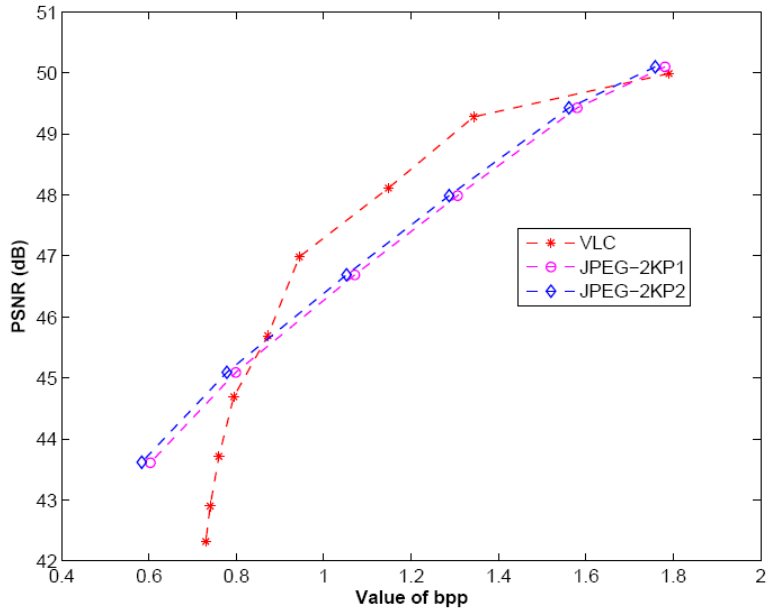

(d)

Figure 10 Comparison of VIF as a function of bit rate (bpp) for visually lossless compression with JPEG 2000 Part 1 (JP-2KP1) and JPEG 2000 Part 2 (JP-2KP2), (a) CT skull (b) CT wrist (c) MRI liver t1 (d) MRI Ped chest (see online version for colours)

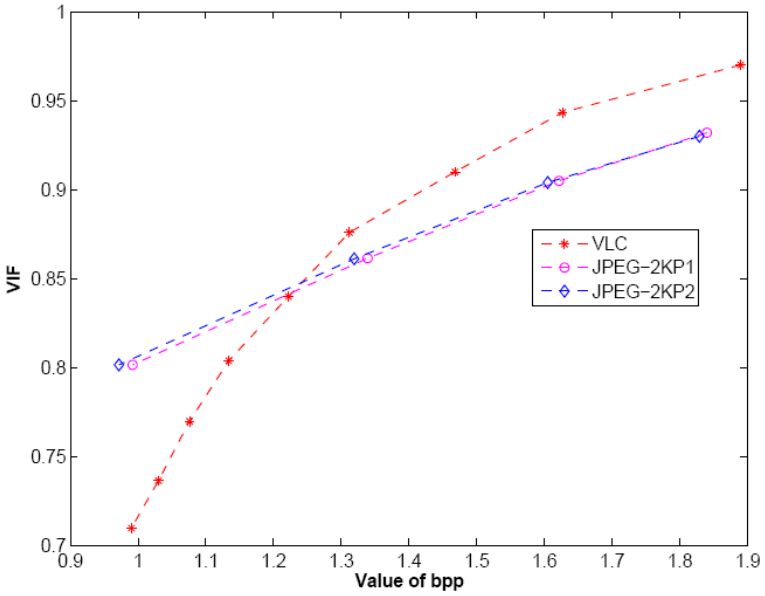

(a)

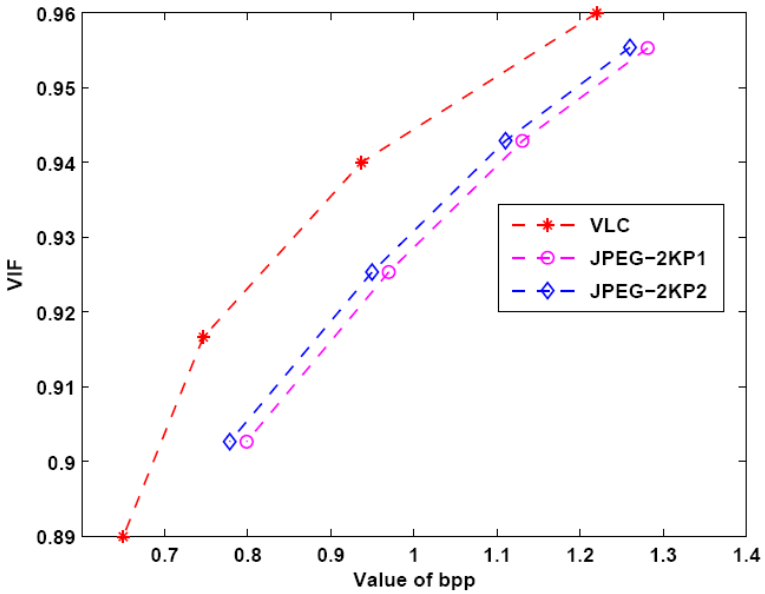

(b)

Figure 10 Comparison of VIF as a function of bit rate (bpp) for visually lossless compression with JPEG 2000 Part 1 (JP-2KP1) and JPEG 2000 Part 2 (JP-2KP2), (a) CT skull (b) CT wrist (c) MRI liver t1 (d) MRI Ped chest (continued) (see online version for colours)

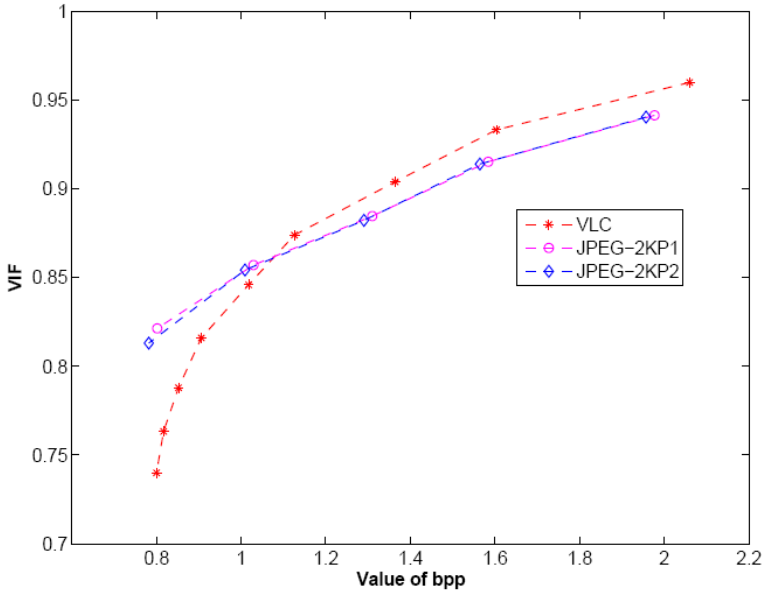

(c)

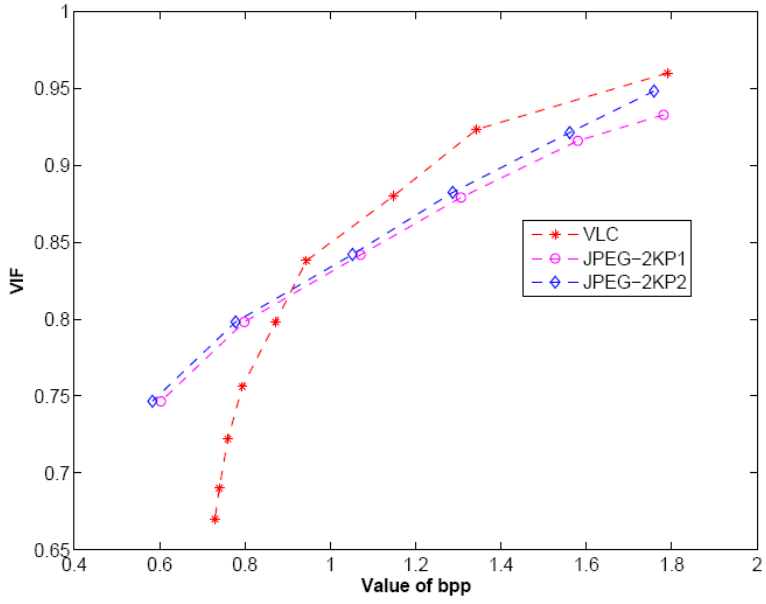

(d)

Figure 11 Comparison of SSIM as a function of bit rate (bpp) for visually lossless compression with JPEG 2000 Part 1 (JP-2KP1) and JPEG 2000 Part 2 (JP-2KP2), (a) CT skull (b) CT wrist (c) MRI liver t1 (d) MRI Ped chest (see online version for colours)

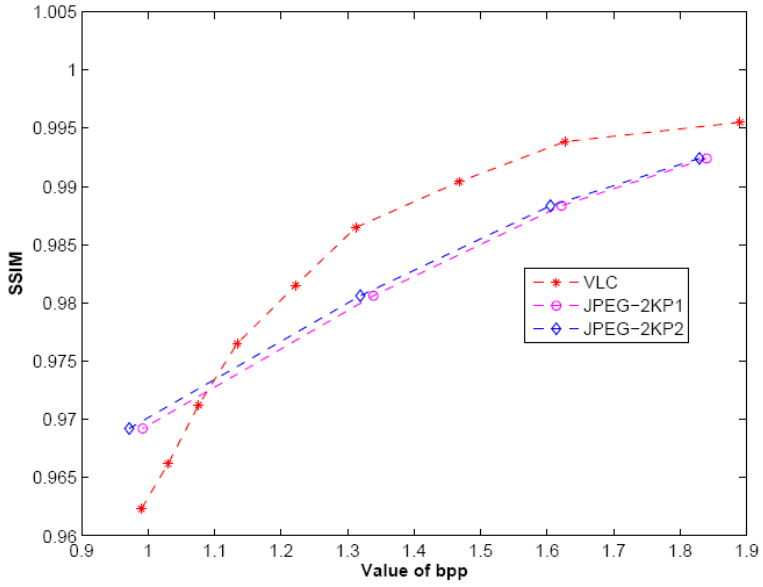

(a)

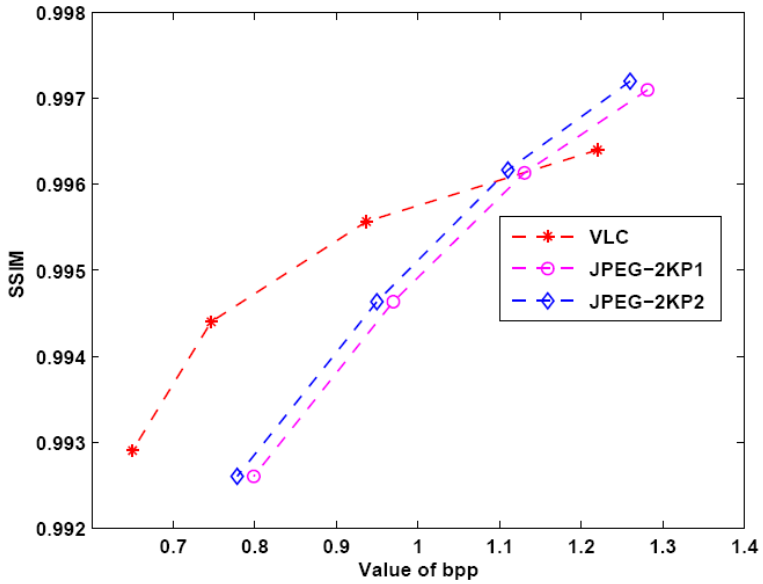

(b)

Figure 11 Comparison of SSIM as a function of bit rate (bpp) for visually lossless compression with JPEG 2000 Part 1 (JP-2KP1) and JPEG 2000 Part 2 (JP-2KP2), (a) CT skull (b) CT wrist (c) MRI liver t1 (d) MRI Ped chest (continued) (see online version for colours)

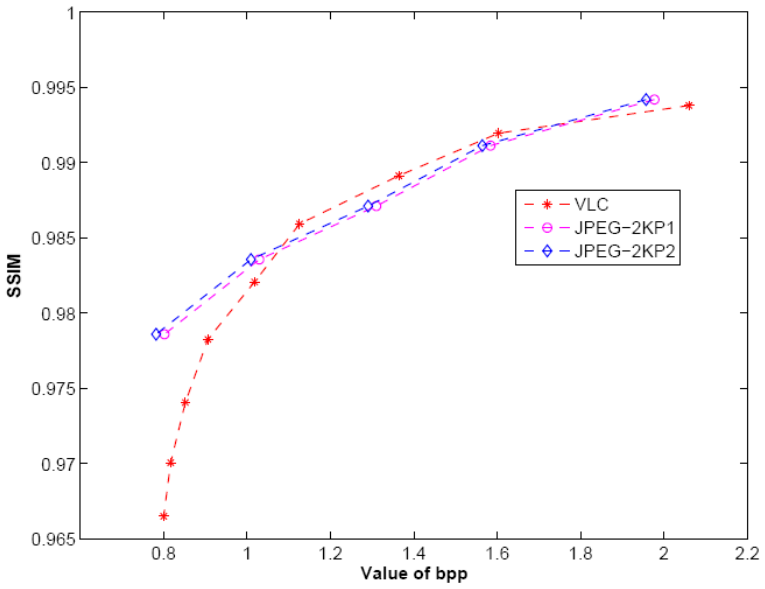

(c)

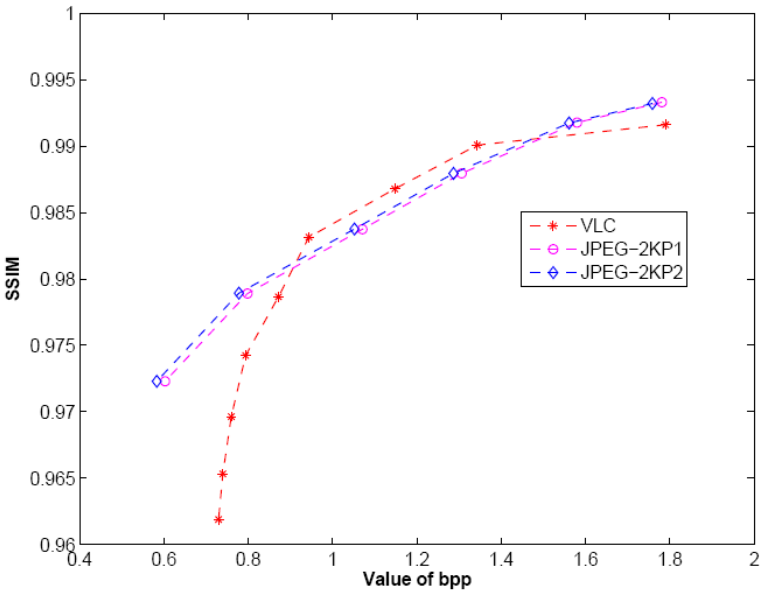

(d)

5.6 Rate-distortion performance

We performed the simulation to get quality of reconstructed image at various bit rates. Here, visually lossless bit rates are calculated considering only one value of k at a time (Figure 3). PSNR in dB, VIF values were determined as a function of bit rate. Since SSIM provides the best performance indicator and it gives the closest match to the subjective quality (Kowalik-Urbaniak et al., 2014), SSIM quality measure also considered. Obtained rate-distortion performance is compared with JPEG-2K Part 1 and JPEG-2K Part 2. We used Kakadu 7.4 version software for the implementation of JPEG-2KP1 and JPEG-2KP2 (KAKADU). Figure 8 shows reconstructed images with our VLC for the selected image slices at different bit rates. Figure 9, Figure 10 and Figure 11 show that proposed coder achieves higher quality measures for a reasonable range of bit rates.

6 Conclusions

Lossless compression techniques are preferred by radiologists as they provide perfect reconstruction, even though they fail to provide good compression ratio. Although lossy compression techniques improve the compression ratio, discarding any information in the medical data could affect the diagnosis. So a new visually lossless approach is proposed in this paper as an alternative solution to lossless and lossy techniques providing good compression ratio and visual quality.

Proposed VLC for 3D MRI and CT medical images incorporates wavelet-based visual model to identify visually irrelevant information, JND dependent quantiser to eliminate them and block match scheme to remove slice redundancy. The performance of the proposed algorithm was compared with that of pixel-based visually lossless compression technique and other lossless standard compression codecs such as JPEG-LS, JPEG-2000, JPEG-3D, H.264/MPEG-4AVC, DPCM and MILC. Results demonstrate that the proposed coder performs better and there is no degradation in visual quality of reconstructed image.

Acknowledgements

The authors would like to thank Professor A. Bilgin, Department of Electrical and Computer Engineering, University of Arizona, Tucson, USA for providing us the medical image datasets. Also, we thank Mr. Saharsh Oza, Department of Electronics and Communication Engineering, NITK Surathkal for helping us in evaluating the compression ratios obtained for the MRI and CT datasets with standard image and video codecs.

References

Adams, M.D. and Ward, RW. (2001) 'Wavelet transforms in the JPEG-2000 standard', *Proc. of IEEE Pacific Rim Conference on Communications, Computers and Signal Processing*, Victoria, BC, Canada, Vol. 1, pp.160–163.

Ait-Aoudia, S., Benhamida, F.Z. and Yousfi, M.A. (2006) 'Lossless compression of volumetric medical data', *International Symposium on Computer and Information Sciences*, pp.563–571.

Amraee, S., Karimi, N., Samavi, S. and Shirani, S. (2011) 'Compression of 3D MRI images based on symmetry in prediction-error field', *IEEE International Conference on Multimedia and Expo*, pp.1–6.

Bilgin, A., Zweig, G. and Marcellin, M.W. (2000) 'Three-dimensional image compression with integer wavelet transforms', *Applied Optics*, Vol. 39, No. 11, pp.1799–1814.

Chandler, D.M. and Hemami, S.S. (2007) 'VSNR: a wavelet-based visual signal-to-noise ratio for natural images', *IEEE Transactions on Image Processing*, Vol. 16, No. 9, pp.2284–2298.

Chandrika, B.K., Aparna, P. and Sumam, D.S. (2014) 'Symmetry based perceptually lossless compression of 3D medical images in spatial domain', *IEEE International Conference on Computer, Communications, and Control Technology*, pp.53–57.

Chou, C-H. and Li, Y-C. (1995) 'A perceptually tuned subband image coder based on the measure of just-noticeable-distortion profile', *IEEE Transactions on Circuits and Systems for Video Technology*, Vol. 5, No. 6, pp.467–476.

Gaudeau, Y. and Moureaux, J.M. (2009) 'Lossy compression of volumetric medical images with 3D dead-zone lattice vector quantization', *Annals of Telecommunications*, Vol. 64, No. 5, pp.359–367.

JPEG2ISO: International Organization for Standardisation (1999) ISO/IEC JTC1/SC29/WG1 N1420: JPEG2000 Verification Model 5.0 Tech. Description, USA, ISO.

JPEG3DISO: International Organization for Standardisation (2002) ISO/IEC15 444-2: Information Technology-JPEG2000 Image Coding System-Part 2: Extensions, USA, ISO.

Kowalik-Urbaniak, I., Brunet, D., Wang, J., Koff, D., Smolarski-Koff, N., Vrscay, E.R., Wallace, B. and Wang, Z. (2014) 'The quest for diagnostically lossless medical image compression: a comparative study of objective quality metrics for compressed medical images', *SPIE Medical Imaging*, pp.903717–903717.

Liu, Z., Karam, L.J. and Watson, A.B. (2006) 'JPEG2000 encoding with perceptual distortion control', *IEEE Transactions on Image Processing*, Vol. 15, No. 7, pp.1763–1778.

Loy, G. and Eklundh, J-O. (2006) 'Detecting symmetry and symmetric constellations of features', *Computer Vision – ECCV*, pp.508–521.

Marpe, D., Wiegand, T. and Sullivan, G.J. (2006) 'The H. 264/MPEG4 advanced video coding standard and its applications', *IEEE Communications Magazine*, pp.134–143.

Menegaz, G. and Thiran, J.P. (2003) 'Three-dimensional encoding/two-dimensional decoding of medical data', *IEEE Transactions on Medical Imaging*, Vol. 22, No. 3, pp.424–440.

Pizzolante, R. and Carpentieri, B. (2013) 'Lossless, low-complexity, compression of three-dimensional volumetric medical images via linear prediction', *IEEE 18th International Conference on Digital Signal Processing*, pp.1–6.

Ramaswamy, A. and Mikhael, WB (1996) 'A mixed transform approach for efficient compression of medical images', *IEEE Transactions on Medical Imaging*, Vol. 15, No. 3, pp.343–352.

Sanchez, V., Abugharbieh, R. and Nasiopoulos, P. (2009a) '3D scalable lossless compression of medical images based on global and local symmetries', *16th IEEE International Conference on Image Processing*, pp.2525–2528.

Sanchez, V., Abugharbieh, R. and Nasiopoulos, P. (2009b) 'Symmetry-based scalable lossless compression of 3D medical image data', *IEEE Transactions on Medical Imaging*, Vol. 28, No. 7, pp.1062–1072.

Sheikh, H.R. and Bovik, A.C. (2006) 'Image information and visual quality', *IEEE Transactions on Image Processing*, Vol. 15, No. 2, pp.430–444.

Tzannes, A. (2003) *Compression of 3-Dimensional Medical Image Data Using Part 2 of JPEG 2000*, Inc. ISO/IEC JTC1/SC29/WG1, Vol. 1.

Villasenor, J.D., Belzer, B. and Liao, J. (1995) 'Wavelet filter evaluation for image compression', *IEEE Transactions on Image Processing*, Vol. 4, No. 8, pp.1053–1060.

Wang, Z., Bovik, A.C., Sheikh, H.R. and Simoncelli, E.P. (2004) 'Image quality assessment: from error visibility to structural similarity', *IEEE Transactions on Image Processing*, Vol. 13, No. 4, pp.600–612.

Watson, A.B., Yang, G.Y., Solomon, J. and Villasenor, J. (1997) 'Visibility of wavelet quantization noise', *IEEE Transactions on Image Processing*, Vol. 6, No. 8, pp.1164–1175.

Weinberger, M.J., Seroussi, G. and Sapiro, G. (2000) 'The LOCO-I lossless image compression algorithm: principles and standardization into JPEG-LS', *IEEE Transactions on Image Processing*, Vol. 9, No. 8, pp.1309–1324.

Wu, D., Tan, D.M., Baird, M., DeCampo, J., White, C. and Wu, H.R. (2006) 'Perceptually lossless medical image coding', *IEEE Transactions on Medical Imaging*, Vol. 25, No. 3, pp.335–344.

Yang, XK., Ling, WS., Lu, Z.K., Ong, E.P. and Yao, SS. (2005) 'Just noticeable distortion model and its applications in video coding', *Signal Processing: Image Communication*, Vol. 20, No. 7, pp.662–680.

Websites

H.264/AVC Reference Software [online] http://iphome.hhi.de/suehring/tml/download/ (accessed 15 January 2015).

JPEG 2000: Openjpeg, Open Source C-libary for JPEG 2000 [online] https://code.google.com/p/openjpeg/wiki/Downloads?tm=2 (accessed 15 January 2015).

JPEG 3D, Open Source C-libary for JPEG 3D [online] https://code.google.com/p/openjpeg/downloads/ (accessed 15 January 2015).

JPEG-LS: Reference Encoder – V.1.00 [online] http://www.hpl.hp.com/loco (accessed 20 January 2015).

KAKADU: Version 7.4 JPEG2000 Software Development Tool Kit [online] http://kakadusoftware.com/ (accessed 15 January 2015).